EXPERIMENTAL ANALYSIS OF MIXED CONVECTION HEAT TRANSFER ON HEAT SINK OF LED LAMP

Sheng-Chung Tzeng and Tzer-Ming Jeng
Department of Mechanical Engineering, Chienkuo Technology University, Changhua County, 500, Taiwan
E-mail: tsc@ctu.edu.tw; tmjeng@cc.ctu.edu.tw

ICETI 2012-G2002_SCI
No. 13-CSME-55, E.I.C. Accession 3513

ABSTRACT

The device made of fan and pin-fin heat sink should be a powerful heat sink for LED lamp. This study used transient liquid crystal experimentation to measure the end-wall heat transfer coefficient of linearly arrayed square pin array in the rectangular channel, and discussed the influence of longitudinal spacing on heat transfer. The relative transverse spacing ($X_T = S_T/d$) was set as 3, and the relative longitudinal spacing ($X_L = S_L/d = 1.88$–5) and the Reynolds number (Re = 11047–17937) were changed. Considering the end-wall area, the average Nusselt number with square pin was 1.46–2.58 times of that without square pin, and the square pin array of $X_L = 3.75$ had the maximum end-wall heat transfer gain.

Keywords: pin-fin heat sink; LED; end-wall heat transfer; longitudinal spacing.

ANALYSE EXPÉRIMENTALE DU TRANSFERT THERMIQUE DE CONVECTION MIXTE POUR DISSIPATEUR DE CHALEUR DANS UNE LAMPE DEL

RÉSUMÉ

Le dispositif fait d'un ventilateur et d'un dissipateur de chaleur pourvu d'ailettes à broches devrait être un dissipateur thermique très efficace dans une lampe DEL. Cette recherche utilise en expérimentation des cristaux liquides transitoires, pour mesurer le coefficient de transfert thermique aux extrémités des parois, disposés de façon linéaire en une rangée de tiges carrées dans le canal rectangulaire. On discute de l'influence de l'espacement longitudinal sur le transfert thermique. L'espacement transversal ($X_T = S_T/d$) est réglé à 3, et l'espacement longitudinal ($X_L = S_L/d = 1.88$–5) et le nombre Reynolds (Re = 11047–17937) ont été changés. En considérant l'extrémité de la paroi, le nombre Nusselt moyen avec tiges carrées est de 1.46–2.58 fois celui sans tiges carrées, et la rangée de tiges carrées de $X_L = 3.75$ montre le gain maximum de transfert thermique aux extrémités des parois.

Mots-clés : dissipateur thermique à ailettes à broches ; DEL ; transfert thermique aux extrémités des parois ; espacement longitudinal.

NOMENCLATURE

A_{EW}	end-wall area (m^2)
d	side length of the square pin fin (m)
D_h	hydraulic diameter of the test channel (m)
h	heat transfer coefficient ($W/m^2/K$)
H	height of the test channel (m)
H_f	height of the pin fin (m)
k	thermal conductivity (W/m/K)
Nu	Nusselt number
$\overline{\text{Nu}}$	average Nusselt number
Re	Reynolds number
L	length of the test channel (m)
S_L	longitudinal spacing (m)
S_T	transverse spacing (m)
T	temperature (°C)
U	average velocity of air (m/s)
W	width of the test channel (m)
W^*	channel width excluding pin fins (m)
x	longitudinal axis (m)
X_L	relative longitudinal spacing
X_T	relative transverse spacing
Greek symbols	
α	thermal diffusion coefficient (m^2/s)
μ	viscosity (kg/m/s)
ρ	density (kg/m^3)
Subscripts	
0	initial condition or without pin fin
b	bulk mean temperature
f	fluid
g	liquid crystal changed to green
i	at the inlet
o	at the outlet
w	wall

1. INTRODUCTION

At present, the demand for precision and minniaturization of electronic equipments has led to the demand for the miniaturization, high power, high density and high efficiency of electronic modules. The electronic modules can thus generate heat inevitably in the working process, and the heat must be cooled down by the heat sinking module, so as to avoid too high temperature of electronic modules influencing the stability and reliability of products. The pin-fin array is a common heat sink configuration. Combining the fan and pin-fin heat sink may be a powerful cooling device for LED lamp, such as shown in Fig. 1. The pin-fin arrangement mode and spacing (including longitudinal and transverse spacing) influence the partial and overall heat transfer significantly. Many scholars have discussed this forced convection heat transfer problem, but most of them focus on the heat exchange between pin-fin surface and cold flow. As for the end-wall heat transfer characteristics of wall surface shooting pin-fins, most of previous studies discussed the heat flow characteristics of end-wall around single pin-fin [1–5], and found that when the fluid impacted the pin-fins, the vortex systems such as Horseshoe Vortex, Corner Vortex and Counter Vortex were generated

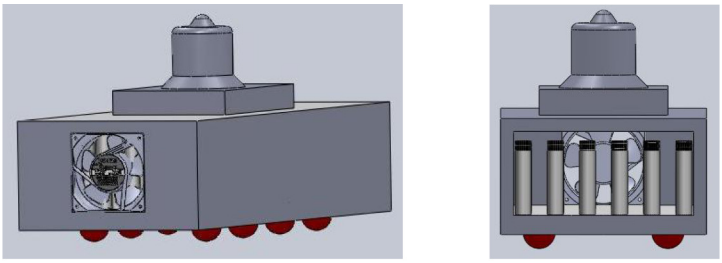

Fig. 1. Sketch map of pin-fin heat sink for LED lamp.

around the pin-fins (see Fig. 1).

Sparrow et al. [1] experimentally studied the heat transfer characteristics near the root of single circular pin-fin, and used flow field observation technique to observe the characteristics of Horseshoe Vortex system. They found that the range influenced by the vortex system was within 1 circular pin diameter above the pin-fin root, and the heat transfer in this range was lower than that of the uninfluenced pin-fin surface by about 9% on average. Igarashi [2] experimentally studied the influence of different attack angles and different depth-width ratios of square pin on the local and average heat transfer coefficients of square pin surface. He proposed the relationships of various surface Nusselt numbers of cube at different attack angles and different depth-width ratios. Chyu and Natarajan [3] used volatilization mass transfer to prove the influence of Horseshoe Vortex and Corner Vortex on the mass transfer coefficients around the cube surface. The results showed that the average mass transfer coefficient of the cube side was the maximum value because of the Horseshoe Vortex. Chyu and Natarajan [4] studied the geometric shapes of different prominences. The results showed that the upstream horseshoe vortex system of prominence and the Arch-Shaped Vortex behind the prominence were resulted from the interaction between prominence and substrate, and the reattachment length behind the prominence was as follows: diamond, cube, circular pin, triangle pyramid and hemicycle. Yoo et al. [5] discussed the influence of square pin at different attack angles on the mass transfer coefficient of substrate surface. They found that when the attack angle was 12–13°, the average mass transfer coefficient of substrate surface was at its minimum, whereas when it was 20–25°, the average mass transfer coefficient of substrate surface was at its maximum. Hwang and Lui [6, 7], Tanda [8], Wierzbowski and Stasiek [9], Kim et al. [10] and Won et al.[11] investigated the end-wall heat transfer of the channel filled with pin-fin array. The pin-fin array is widely used in the cooling design of the electronic equipments and the blades of turbine. The heat-exchange surfaces of pin-fin array include both the skin surfaces of pin fins and the end wall. The heat transfer characteristics on both surfaces are influenced strongly by the shape, height, arrangement and space of pin fins.

Furthermore, the traditional heat-transfer experiments usually use the thermocouples to measure temperatures. It is difficult to obtain the detailed measurement of heat transfer coefficients. The transient liquid crystal method can easily and quickly complete the detailed measurement of the heat transfer coefficient. Its experimental error due to heat loss is much smaller than the traditional one. Therefore, many studies have employed the transient liquid crystal method to investigate the heat-transfer issues, including cylinder surface [12], curve surface [13, 14], smooth wall channel [15–17], ribbed wall channel [18, 19], film cooling [20], and impinging jet [21, 22].

This work completed the detailed measurement of end-wall heat transfer coefficients of square pin-fin heat sink by the transient liquid crystal method. The air was used as coolant and the transverse space between fins was fixed. The effects of the air flow rate and the longitudinal space between fins on end-wall heat transfer were investigated.

2. EXPERIMENT

2.1. Theory of Transient Liquid Crystal Experiment Method

This study used transient liquid crystal experiment method to measure the heat transfer coefficients. The theoretical model uses hot air to heat the test piece surface coated with liquid crystal, the thickness of the test piece is designed properly, and the test piece is made of material with low heat transfer coefficient. The heat is transferred from the inner wall of the test piece to the outer wall but has not yet reached the outer wall within a short period of time. A one-dimensional semi-infinite field heat conduction problem is formed, and the inner wall temperature can be expressed as

$$\frac{T_w - T_0}{T_{fi} - T_0} = 1 - \exp\left(\frac{h^2 \alpha t}{k^2}\right) \operatorname{erfc}\left(\frac{h\sqrt{\alpha t}}{k}\right) \tag{1}$$

where T_w is the inner wall temperature, T_0 is the initial temperature, T_{fi} is the inlet air temperature, k is the thermal conductivity of wall, α is the thermal diffusion coefficient of wall, h is the heat transfer coefficient of air for the test wall, t is the time. Therefore, as long as the thermal properties of test wall and related temperatures and wall temperature at special time are given, the heat transfer coefficient (h) value can be obtained by using Eq. (1). The air inlet temperature is not presented as a perfect step function in the testing process (current heating unit cannot make it), but rises sharply with time at the beginning, and then becomes gentle and constant. Therefore, the air inlet temperature (T_{fi}) will be divided into many consecutive step functions to form actual temperature change. The superposition theory of Duhamel is used, and Eq. (1) can be converted into

$$T_w - T_0 = \sum_{j=1}^{N} \left[1 - \exp\left(\frac{h^2 \alpha (t - \tau_j)}{k^2}\right) \operatorname{erfc}\left(\frac{h\sqrt{\alpha (t - \tau_j)}}{k}\right)\right] [\Delta T_r]. \tag{2}$$

2.2. Experimental Equipments

The experimental system used in this study (as shown in Fig. 2) consists of four parts: (1) the hot air supply system; (2) the test section; (3) the image capture system; and (4) the temperature capture system. The air is blown into the air conduit by the blower, and the frequency converter regulates the motor speed of blower to control the air flow rate. The air velocity is measured by the anemometer. The air is rectified, then delivered to the heater for heating, and enters the test section. The exit of heater is 45cm away from the front edge of test section. Finally, the air is discharged out of the test section. The heater can regulate the heating capacity according to the air flow rate, so as to test the appropriate color changing time of wall surface. The test section is made of 20 mm thick transparent acrylate, the passage section is 120 mm (W) $\times$ 64 mm (H), and the test zone is 240 mm (L) long, above which the 8 mm (d) $\times$ 8 mm (d) $\times$ 64 mm (H_f) square pin-fins are arranged in-line (see Fig. 3). Five columns of square pins are fixed in transverse direction, the relative transverse spacing is $X_T = S_T/d = 3$, and there are 6, 8, 10, 12, 14 and 16 rows of square pins in longitudinal direction respectively, the corresponding relative longitudinal spacing ($X_L = S_L/d$) is 5, 3.75, 3, 2.5, 2.14 and 1.88, respectively. The liquid crystal is sprayed over the channel bottom wall of the test section, and then the black paint is sprayed. The liquid crystal is transparent at room temperature, and it begins to change color when it is heated by hot air to a certain temperature (red, green and blue in turn). Finally, it becomes transparent again, and changes color in reverse order when it is being cooled. The discoloration process is reversible and repeated. The liquid crystal used in this study changed to green and reached 90% strength at the temperature (T_g) of 38.7°. The rise process of air temperature at the test zone entrance is measured by thermocouple and sent to the data recorder (MX100) and turned into temperature value. The whole temperature change process is recorded and stored in computer as input parameter for follow-up analysis of heat transfer coefficients. The image capture equipment shoots the discoloration process of heated liquid

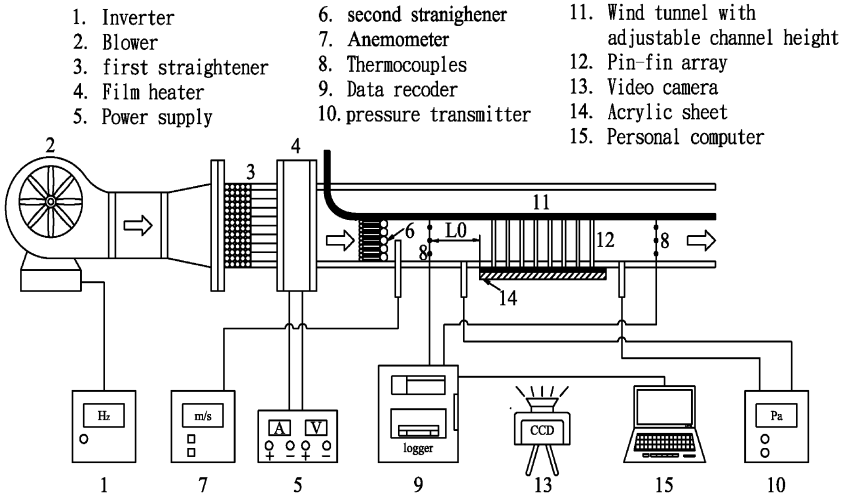

Fig. 2. Experimental setup.

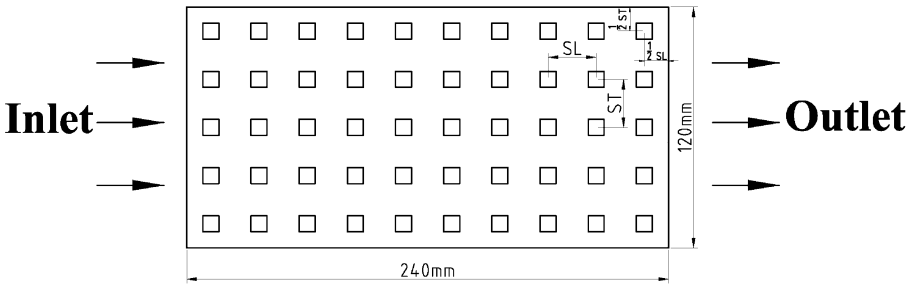

Fig. 3. The dimensions and arrangement of pin fins.

crystal on the channel wall when the hot air has entered the test zone, and the image file can be used for analyzing the time t for liquid crystal to be heated from initial temperature T_0 to T_g (specific temperature at which the liquid crystal turns to green). The camera records the whole process from air heating to the completion of liquid crystal discoloration. The liquid crystal discoloration time in different positions of the test wall can be obtained using commercial software LCIA to analyze the image file, as well as using the air temperature change measured at the test zone entrance. The LCIA software can figure out the heat transfer coefficients of different positions of the test wall by using Eq. (2). The LCIA software can analyze the heat-transfer coefficients of different positions of the tested wall surface based on the inlet air temperature (T_{fi}) and the outlet air temperature (T_{fo}) according to Eq. (1), and then obtain the h-value based on T_{fb} according to interpolation.

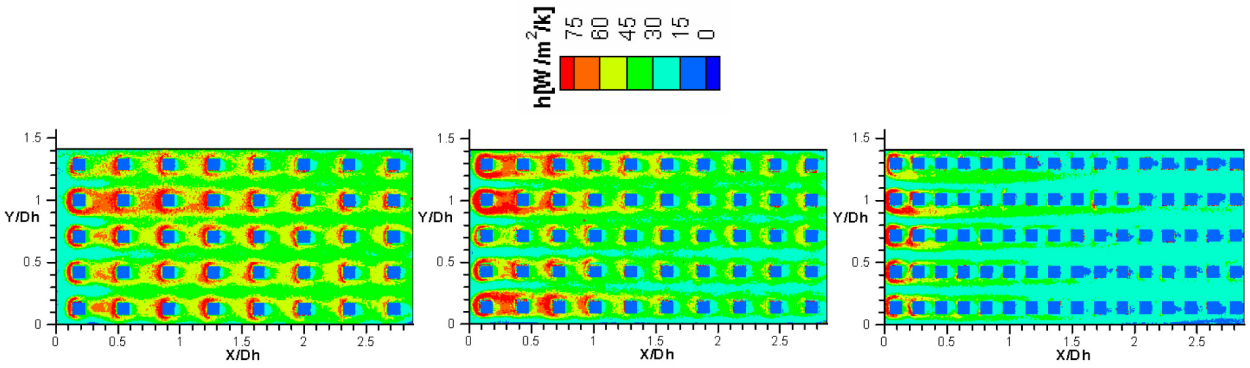

Fig. 4. Contours of heat transfer coefficients (Re = 13970–14667): (a) $X_T = 3$ and $X_L = 3.75$; (b) $X_T = 3$ and $X_L = 3$; (c) $X_T = 3$ and $X_L = 1.88$.

2.3. Data Reduction and Uncertainty Analysis

Related dimensionless parameter Reynolds number (Re) and Nusselt number (Nu and $\overline{\text{Nu}}$) are defined below.

$$\text{Re} = \frac{\rho_f U D_h}{\mu} \tag{3}$$

$$\text{Nu} = \frac{\left[\int_0^W h(x,y)dy\right] D_h}{W^*(x) \cdot k_f} \tag{4}$$

$$\overline{\text{Nu}} = \frac{\left[\int_0^L \int_0^W h(x,y)dydx\right] D_h}{L \cdot W^*(x) \cdot k_f} \tag{5}$$

where ρ_f is the air density, U is the air average velocity, D_h is the hydraulic diameter of the wind channel, μ is the air viscosity, h is the heat transfer coefficient, k_f is the air thermal conductivity, and $W^*(x)$ is the channel width excluding pin fins. The maximum value of $W^*(x)$ is the width of the empty channel (W) and the minimum one is ($W - 3d$). The uncertainty analysis of this experiment adopts Moffat [23] uncertainty analysis method. The uncertainties of Reynolds number (Re), heat transfer coefficient (h) and average Nusselt number ($\overline{\text{Nu}}$) in this experiment are $\pm 2.75\%$, $\pm 7.30\%$ and $\pm 8.96\%$ respectively.

3. RESULTS AND DISCUSSION

As past studies have proposed complete research findings on the forced convection heat transfer inside straight channel, this study compared the measured data of straight channel configuration with previously published findings to validate the correctness of experiment. At present, the distribution of Nusselt number of rectangular channel in the flow direction reasonably coincides with the data of Kuo and Hwang [24] and Dittu and Boelter [25], proving the rationality of this experimental measurement result. Figure 4 shows the heat-transfer coefficient distribution of $X_L = 3.75$, 3 and 1.88 square pin arrays when Re = 13970–14667. The results suggested that there is horseshoe high heat transfer zone at the front windward side of square pins. This feature is the heat transfer capacity enhanced under the influence of Horseshoe vortex, the vortex system develops downstream along both sides of pin-fins, and interacts on main flow and the strength decreases gradually. The Horseshoe Vortex is derived from the air flow interaction as the wall surface boundary layer impacts the front side of pin-fin, generally the range of influence of this vortex on

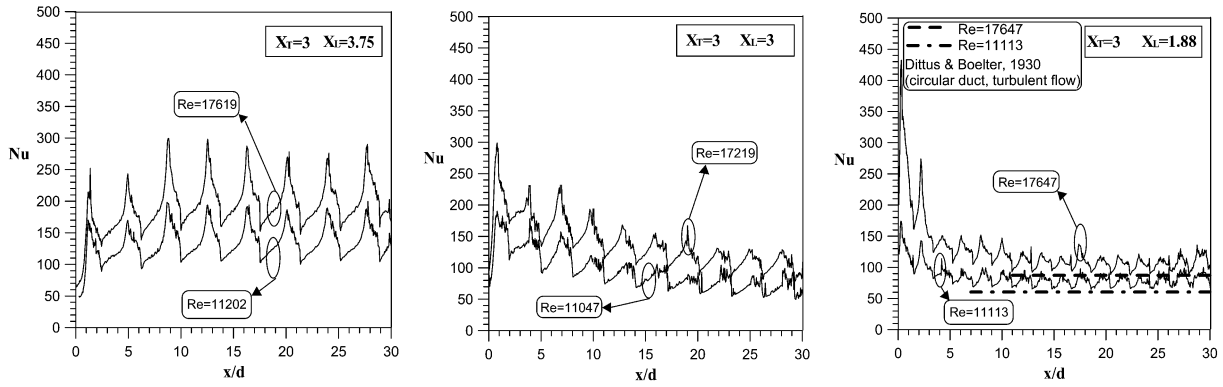

Fig. 5. Transverse average Nusselt number along the longitudinal direction: (a) $X_T = 3$ and $X_L = 3.75$; (b) $X_T = 3$ and $X_L = 3$; (c) $X_T = 3$ and $X_L = 1.88$.

the pin-fin impact surface is from the root to upward d, and there is Counter Vortex at the joint between pin-fin root and wall surface [1–5]. When the relative longitudinal spacing (X_L) is large, the air can impact the square pin and then separate, recombine, and impact the next row of square pins, because even if the lower square pin row can have remarkable Horseshoe Vortex. However, when the relative longitudinal spacing (X_L) is small, as the pin-fins are arranged tightly, the air flow strength in transverse direction is weak. It is thus difficult to be combined completely again after impacting the front row of square pins, so that most of air flows through the longitudinal passage between adjacent rows of pin-fins. Therefore, the downstream square pin row cannot form strong Horseshoe Vortex system, and the downstream heat transfer coefficient is smaller.

Figure 5 shows the distribution of transverse average Nusselt number (Nu) in flow direction (x/d). As seen, the Nu increases fast as approaching to the front edge of square pin row, the peak value occurs at the front edge of square pin row, and then decreases gradually. The rear edge of square pin row has local minimum, similar Nu variation occurs in each square pin row. In the $X_L \geq 3.75$ system, the Nu variation begins to repeat since the third square pin row, and the Nu peak values of the first and the second square pin rows are lower, because the transverse average Nusselt number (Nu) is influenced by the forced convection in the channel between square pin rows and the Horseshoe Vortex system. As the boundary layer of upstream flow field of test zone has developed completely, the Horseshoe Vortex systems of the first and the second square pin rows are stronger, but the forced convection in the channel between square pin rows is weaker. However, the boundary layer developed by upstream flow field behind the third square pin row is destroyed by the square pin array, so the corresponding Horseshoe Vortex system is weaker. The forced convection in the channel between square pin rows becomes stronger, and the longitudinal spacing of $X_L \geq 3.75$ is large enough, so the flow field around square pin row changes repeatedly since the third row. When the X_L decreases continuously (e.g. $X_L \leq 3$), as the longitudinal array of pin-fins is tight, the flow strength of air in transverse direction decreases, so that the air flow has an opportunity to develop on the boundary layer of the channel between square pin rows, then the corresponding Horseshoe Vortex system of downstream square pin row is weakened, and the forced convection in the channel between square pin rows becomes weaker. Therefore, the Nu peak values of various square pin rows decrease gradually with x/d, and then incline to fixed value (fully developed flow is completed). The most ultimate example of close longitudinal array of pin-fins is no spacing in longitudinal direction. At this point, there is only forced convection in the channel between pin-fin rows. The circular pipe fully developed turbulence Nusselt number empirical equation of Dittus and Boelter [25] is used to simulate the Nusselt number of rectangular channel between pin-fin rows, and the data are drawn in the example of $X_L = 1.88$ in Fig. 5, reasonable correlation is found.

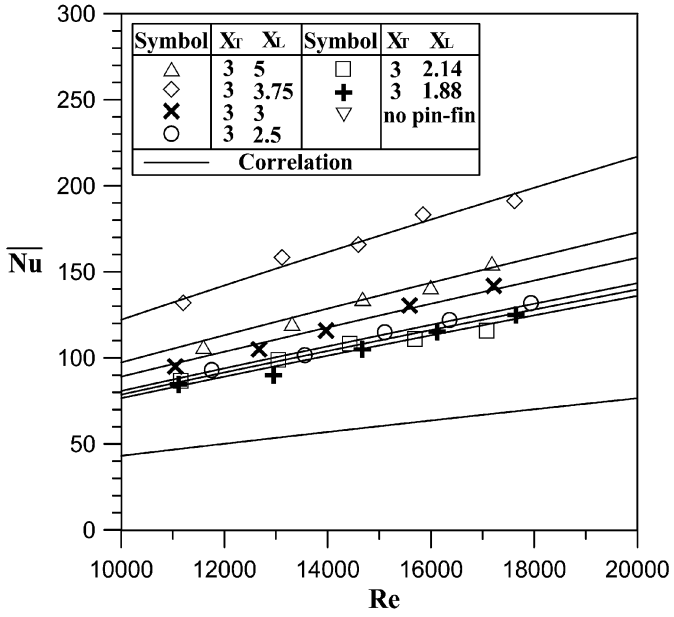

Fig. 6. $\overline{\mathrm{Nu}}$ as a function of Re.

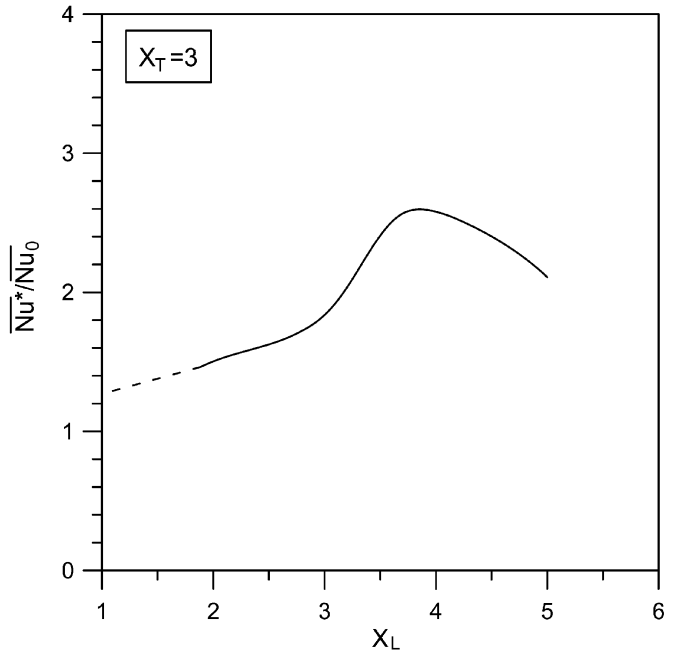

Fig. 7. $\overline{\mathrm{Nu}}$ as a function of X_L.

Figure 6 shows the relation between $\overline{\mathrm{Nu}}$ and Re, when $X_T = 3$, $X_L = 5$–1.88, $X_L = 3.75$ has the best $\overline{\mathrm{Nu}}$, secondly when $X_L = 5$, the worst system is $X_L = 2.5$–1.88, but they are remarkably better than that without square pins, the empirical equation of $\overline{\mathrm{Nu}}$ and Re can be induced from all the experimental data:

$$\overline{\mathrm{Nu}} = A \cdot \mathrm{Re}^{0.829} \tag{6}$$

where $A = 0.047$, 0.059, 0.043, 0.039, 0.038, 0.037 and 0.0208 correspond to $X_L = 5$, 3.75, 3, 2.5, 2.14, 1.88 and no pin-fin respectively.

Figure 7 shows the relation between $\overline{\mathrm{Nu}}^*/\overline{\mathrm{Nu}}_0$ and X_L, where $\overline{\mathrm{Nu}}^*$ is $\overline{\mathrm{Nu}}$ multiplied by $A_{\mathrm{EW}}/L/W$, A_{EW} is the end-wall area, and $\overline{\mathrm{Nu}}_0$ is the average Nusselt number without pin-fin. The result showed that the average Nusselt number with square pin is 1.46–2.58 times of that without square pin, the square pin array of $X_L = 3.75$ has the maximum end-wall heat transfer gain. The end-wall heat transfer gain of the sheet pin-fin array without spacing in longitudinal direction is estimated at 1.27 times of that without pin-fin by the empirical equation of Nusselt number of Dittus and Boelter [25].

4. CONCLUSIONS

This study successfully used transient liquid crystal experimentation to measure the detailed heat transfer coefficient of end-wall in rectangular channel of linearly arrayed square pin array, the relative transverse spacing ($X_T = S_T/d$) was set as 3, and the relative longitudinal spacing ($X_L = S_L/d = 1.88$–5) and Reynolds number (Re = 11047–17937) were changed. Considering the end-wall area, the average Nusselt number with square pin was 1.46–2.58 times of that without square pin, and the square pin array of $X_L = 3.75$ had the maximum end-wall heat transfer gain.

ACKNOWLEDGEMENTS

The authors would like to thank the National Science Council of the Republic of China for financially supporting this research under Contract Nos. NSC 100-2221-E-270-014-MY3, NSC 100-2632-E-270-001-MY3, and NCS 102-2221-E-270-003. Appreciation is given to Mr. Yong-Zhou Chen for his assistance in collecting the experimental data and preparing the graphic drafts.

REFERENCES

1. Sparrow, E.M., Stahl, T.J. and Traub, P., "Heat transfer adjacent to the attached end of a cylinder in crossflow", *Int. J. Heat Mass Transfer*, Vol. 27, pp. 233–242, 1984.
2. Igarashi, T., "Heat transfer from a square prism to an air stream", *Int. J. Heat Mass Transfer*, Vol. 28, pp. 175–181, 1985.
3. Chyu, M.K. and Natarajan, V., "Local heat/mass transfer distributions on the surface of a wall-mounted cube", *ASME J. Heat Transfer*, Vol. 113, pp. 851–857, 1991.
4. Chyu, M.K. and Natarajan, V., "Heat transfer on the base surface of three-dimensional protruding elements", *Int. J. Heat Mass Transfer*, Vol. 39, pp. 2925–2935, 1996.
5. Yoo, S.Y., Goldstein, R.J. and Chung, M.K., "Effects of angle of attack on mass transfer from a square cylinder and its base plate", *Int. J. Heat Mass Transfer*, Vol. 36, pp. 371–381, 1993.
6. Hwang, J.J. and Lui, C.C., "Detailed heat transfer characteristic comparison in straight and 90-deg turned trapezoidal ducts with pin-fin arrays", *Int. J. Heat Mass Transfer*, Vol. 42, pp. 4005–4016, 1999.
7. Hwang, J.J. and Lui, C.C., "Measurement of endwall heat transfer and pressure drop in a pin-fin wedge duct", *Int. J. Heat Mass Transfer*, Vol. 45, pp. 887–889, 2002.
8. Tanda, G., "Heat transfer and pressure drop in a rectangular channel with diamond-shaped elements", *Int. J. Heat Mass Transfer*, Vol. 2001, pp. 3529–3541, 2001.
9. Wierzbowski, M. and Stasiek, J., "Liquid crystal technique application for heat transfer investigation in a fin-tube heat exchanger element", *Exp. Thermal Fluid Sci.*, Vol. 26, pp. 319–323, 2002.
10. Kim, T., Hodson, H.P. and Lu, T.J., "Fluid-flow and endwall heat-transfer characteristics of an ultralight lattice-frame material", *Int. J. Heat Mass Transfer*, Vol. 47, pp. 1129–1140, 2004.
11. Won, S.Y., Mahmood, G.I. and Ligrani, P.M., "Spatially-resolved heat transfer and flow structure in a rectangular channel with pin fins", *Int. J. Heat Mass Transfer*, Vol. 47, pp. 1731–1743, 2004.
12. Cooper, T.E., Field, R.J. and Meyer, J.F., "Liquid crystal thermography and its application to the study of convective heat transfer", *ASME J. Heat Transfer*, pp. 442–450, 1975.

13. Camci, C., Kim, K. and Hippensteele, S.A., "A new hue capturing technique for the quantitative interpretation of liquid crystal image used in convective heat transfer studies", *ASME J. Turbomachinary*, Vol. 114, pp. 765–775, 1996.
14. Chan, T.L., Leung, C.W., Jambunathan, K., Ashforth-Frost, S., Zhou, Y. and Liu, M.H., "Heat transfer characteristics of a slot jet impinging on a semi-circular convex surface", *Int. J. Heat Mass Transfer*, Vol. 45, pp. 993–1006, 2002.
15. Gao, X. and Sunden, B., "Detailed measurements of heat transfer coefficients in a rectangular duct using hue-based calibrated liquid crystal", *Int. Comm. Heat Mass Transfer*, Vol. 27, pp. 13–22, 2000.
16. Liou, T.M., Chen, C.C. and Chen, M.Y., "TLCT and LDV measurements of heat transfer and fluid flow in a rotating sharp turning duct", *Int. J. Heat Mass Transfer*, Vol. 44, pp. 1777–1787, 2001.
17. Jeng, T.M., Wang, M.P., Hwang, G.J. and Hung, Y.H., "Thermal behavior in rectangular channels by using transient liquid crystal method", *Exp. Heat Transfer*, Vol. 17, pp. 147–160, 2004.
18. Tanda, G., "Heat transfer in rectangular channels with transverse and V-shaped broken ribs", *Int. J. Heat Mass Transfer*, Vol. 47, pp. 229–243, 2004.
19. Ekkad, S.V. and Han, J.C., "Detailed heat transfer distributions in two-pass square channels with rib turbulators", *Int. J. Heat Mass Transfer*, Vol. 40, pp. 2525–2537, 1997.
20. Falcoz, C., Weigand, B. and Ott, P., "Experimental investigations on showerhead cooling on a blunt body", *Int. J. Heat Mass Transfer*, Vol. 49, pp. 1287–1298, 2006.
21. Wang, T., Lin, M. and Bunker, R.S., "Flow and heat transfer of confined impingement jets cooling using a 3-D transient liquid crystal scheme", *Int. J. Heat Mass Transfer*, Vol. 48, pp. 4887–4903, 2005.
22. Yan, W.M. and Mei, S.C., "Measurement of detailed heat transfer along rib-roughened surface under arrays of impinging elliptic jets", *Int. J. Heat Mass Transfer*, Vol. 49, pp. 159–170, 2006.
23. Moffat, R.J., "Contributions to the theory of single-sample uncertainty analysis", *ASME J. Fluids Engrg.*, Vol. 104, pp. 250–260, 1986.
24. Kuo, C.R. and Hwang, G.J., "Aspect ratio effect on convective heat transfer of radially outward flow in rotating rectangular ducts", *Int. J. Rotating Machinery*, Vol. 1, pp.1–18, 1994.
25. Dittus, P.W. and Boelter, L.M.K., "Heat transfer in automobile radiators of the tubular type, *University of California, Publications in Engineering*, Vol. 2, No. 13 pp. 443–461, 1930; reprinted in *Int. Comm. Heat Mass Transfer*, Vol. 12, pp. 3–22, 1985.